Progress In Electromagnetics Research, Vol. 131, 99–115, 2012

TWO-PHASE LOW CONDUCTIVITY FLOW IMAGING USING MAGNETIC INDUCTION TOMOGRAPHY

H.-Y. Wei and M. Soleimani*

Department of Electronics and Electrical Engineering, University of Bath, U.K.

Abstract—Magnetic Induction Tomography (MIT) is a new and emerging type of tomography technique that is able to map the distribution of all three passive electromagnetic properties, however most of the current interests are focusing on the conductivity and permeability imaging. In an MIT system, coils are used as separate transmitters or sensors, which can generate the background magnetic field and detect the perturbed magnetic field respectively. Through switching technique the same coil can work as transceiver which can generate field at a time and detect the field at another time. Because magnetic field can easily penetrate through the non-conductive barrier, the sensors do not need direct contact with the imaging object. These non-invasive and contactless features make it an attractive technique for many applications compared to the traditional contact electrode based electrical impedance tomography. Recently, MIT has become a promising monitoring technique in industrial process tomography, for example MIT has been used to determine the distribution of liquidised metal and gas (high conductivity two phase flow monitoring) for metal casting applications. In this paper, a low conductivity two phase flow MIT imaging is proposed so the reconstruction of the low contrast samples ($< 6\,\mathrm{S/m}$) can be realised, e.g., gas/ionised liquid. An MIT system is developed to test the feasibility. The system utilises 16 coils (8 transmitters and 8 receivers) and an operating frequency of 13 MHz. Three different experiments were conducted to evaluate all possible situations of two phase flow imaging: 1) conducting objects inside a non-conducting background, 2) conducting objects inside a conducting background (low contrast) and 3) non-conducting objects inside a conducting background. Images are reconstructed using the linearised inverse method with regularisation. An experiment was designed to image the non-conductive samples inside a conducting

Received 6 July 2012, Accepted 17 August 2012, Scheduled 5 September 2012

* Corresponding author: Manuchehr Soleimani (m.soleimani@bath.ac.uk).

background, which is used to represent the size varying bubbles in ionised solution. The temporal reconstruction algorithm is used in this dynamic experiment to improve the image accuracy and noise performance.

1. INTRODUCTION

Magnetic induction tomography (MIT) is one of the electromagnetic tomography techniques that images the spatial distribution of electrical conductivity and magnetic permeability inside a region of interest. Its contactless imaging feature makes it potentially very attractive to both industrial non-destructive testing (NDT) and other process tomography applications. For a typical MIT system, coils are used as the transmitters and receivers based on the mutual inductance theory. By establishing a sinusoidal current into a driving coil, a time varying magnetic flux is set up, which induces a back emf at the sensor coils. This induced voltage generated by the driving magnetic field strength is often referred to as the 'primary' signal [1]. If a conductive object is located in a sensitive enough region, eddy current will be induced on the surface of the object. This eddy current can produce a secondary magnetic field, which will induce a 'secondary' voltage signal and perturb the primary signal at the receiving coil. This perturbation signal is proportional to the object conductivity and will be used to reconstruct the conductivity images.

Two phase flow normally takes place in a system containing a dynamic process which involves both gas and liquid. In recent years, oil & gas companies are particularly interested in knowing the flowing patterns of the process during the system operation. Understanding the mixing, settlement and concentration behavior can improve the understanding of the system performance and hence increase the system efficiency. Beside other commercial systems such as ultrasound, microwave and γ-rays, process tomography techniques such as electrical impedance tomography (EIT) and electrical capacitance tomography (ECT) have actually been widely applied into the many two phase flow imaging applications, for example the oil/gas distribution using ECT (electrical permittivity contrast) [2] and the oil/water distribution using EIT (electrical conductivity contrast) [3]. In recent years, MIT has also been a great success in two phase flow monitoring which involves gas/melting metal flow for metal casting applications, based on the high conductivity contrast between melted metal and gas [4, 5]. Several low and high frequency electromagnetic imaging techniques similar to MIT may provide great monitoring and control opportunities in the field of industrial process

tomography [29–34].

It is believed that MIT could be more suitable for two-phase flow monitoring because of its contactless features, as it is generally difficult and in some cases impossible to attach EIT electrodes onto the measuring samples. Initial two phase MIT studies was reported in [6, 7]. However, the imaging results showed in [7] were mainly simulation and limited two phase imaging result (only conductors inside a freespace background) was demonstrated in [6]. In this paper, more in-depth results and the analysis of low conductivity two phase imaging using contactless MIT are provided to determine the gas/liquid or liquid/liquid distribution (conductivity $< 6\,\mathrm{S/m}$). The eddy current technique has an advantage in that it is sensitive only to the conductive component within the measuring space. ECT can not be utilised in this configuration as there is little permittivity contrast. Because of the very small conductivity contrast, the perturbation signal at the receiving coil will be several orders lower than the signal detected in the metal casting application. This has become one of the greatest challenges for low conductivity MIT imaging. In order to acquire such a small perturbation from the conductivity changes less than 6 S/m, a highly accurate and stable signal source and phase shift measurement MIT hardware are necessary. In this paper, a prototype National Instruments (NI) based system for biomedical MIT applications is used [8] for experimental verification. The system utilises NI products to accomplish all signal driving, switching and data acquisition tasks, which ease the system design whilst providing satisfactory performance.

This paper demonstrates the feasibility of the low conductivity two phase imaging using MIT techniques. Several laboratory experiments were conducted for the first time to model all possible gas/liquid cases. Data is sampled using the developed NI system. After solving the forward and inversion problems, the reconstructed images from the real sample experiments are provided and discussed in the result section.

2. MIT SYSTEM SETUP

The full development process of the MIT hardware and sensors was reported in [8]. The coil sensors utilise the screened cable and the balanced coil structure to eliminate the capacitive coupling. The 6-turn balanced sensor was constructed onto a 4 cm diameter plastic cylindrical former, which provided a resonance frequency of 45 MHz, with a low inductance of 1.8 μH. NI products and LabView are used to centralise all the driving (NI 5781), switching (NI 2593) and data acquisition (NI 5781) tasks of the MIT system, which decrease the

system design complexity and eliminate the synchronisation problem completely. A 16 channel MIT system was assembled, where the channel switching card NI 2593 is configured to the 2×8 : 1 multiplexer scheme, so eight of the sensor coils are dedicated to transmitters and the other eight coils are dedicated to receivers. The transmitters and the receivers are attached in adjacent positions and evenly spread around a 23.5 cm diameter perspex cylinder to ensure the system's symmetry. Figure 1 shows the system's block diagram of the MIT system.

A driving frequency of 13 MHz is chosen for the system operation, which is low enough for avoiding the coil resonance. The quadrature (I/Q) demodulation method is implemented for eddy current signal

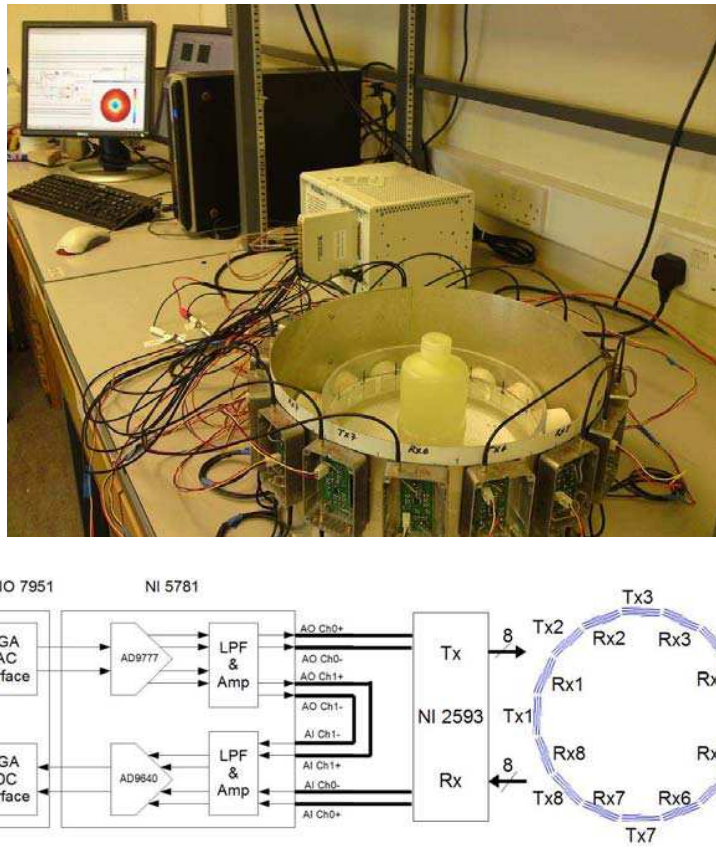

Figure 1. The complete 16 channel MIT system block diagram and the setup for saline bottle detection.

measuring, as it offers a much better measurement stability, with a 40 mV input level, a maximum of 4 m° phase noise can be achieved [8]. The system has the capability of detecting phase shifts that are introduced by the conductivity changes within the measuring space. The hardware performance comparison with other MIT systems and some initial image reconstruction result of the prototype system can be found in [8]. It is known from these initial results that the measurement data is still considered noisy compared to other electrical tomography systems, due to the fact that the low conductivity MIT system is challenging to build and very sensitive to environmental disturbances. There are many possible error sources that can affect the MIT hardware, such us temperature variation, external electromagnetic source, environmental vibration and misalignment of sensors. In [9], it is stated that the geometry mismatch of the sensor can also cause a significant error in terms of the of data deviation, due to the small perturbation signal from the low conductivity contrast. Some of the parameters can be well controlled and compensated when the system is working under a laboratory environment, for example the temperature variation and background noises. However for an industrial MIT system, all these error sources must be re-considered for the future development. An accurate mechanical design is important when the system is working under a real industrial environment. Several error sources can be overcome if the system is provided with a good mechanical support for example the accuracy of sensor's consistency, precision of sensor alignment, external vibration reduction, cooling system design and proper electromagnetic screening. An appropriate calibration procedure also needs to be developed for future system expansion for real life applications.

3. IMAGE RECONSTRUCTION

3.1. Forward Problem — Eddy Current Modeling

The purpose of solving the MIT forward problem is to calculate the measurement signals for a predefined conductivity distribution. In MIT, the forward problems are mainly comprised by the eddy current problems, which are governed by Maxwell's equations [10, 11]. The Biot-Savart Law was used in forward model calculations to avoid the coil discretisation in the mesh. In this case, the accuracy of the Biot-Savart integration becomes very important for ensuring the divergence of the eddy current solution [12]. In the (A, A) formulation by edge

FEM, A_s in the freespace can be defined using Biot-Savart Law

$$B_s = \int \frac{\mu_0}{4\pi} \frac{Idl \times r}{|r|^3} \tag{1}$$

and

$$B_s = \nabla \times A_s, \tag{2}$$

where I is the source current, dl a vector whose magnitude is the length of the differential element of the wire, μ_0 the free space permeability constant, and B_s the integration of the magnetic field along each source current segment. This freespace A_s is defined based on the scale of the designed 16 channel MIT system. By substituting the Maxwell's equations, we get the complete eddy current formula

$$\nabla \times \left(\mu^{-1} \nabla \times A_e\right) + j\omega\sigma A_e = \nabla \times H_s - \nabla \times \frac{\mu_0}{\mu} H_s - j\omega\sigma A_s, \tag{3}$$

where σ is the conductivity distribution within the eddy current domain, ω the operational frequency, A_e the reduced potential inside the eddy current region which includes the gradient of the electric scalar potential, and the right hand side is the current density in the excitation coil which is defined based on the freespace components A_s and B_s. Applying Equation (3) into the Galerkin's approximation using edge element basis function [13–15] can yield

$$\begin{aligned} &\int_{\Omega_e} \left(\nabla \times N \cdot \mu^{-1} \nabla \times A_e\right) dv + \int_{\Omega_e} \left(j\omega\sigma N A_e\right) dv \\ &= \int_{\Omega_n} \nabla \times N \cdot H_s dv - \int_{\Omega_n} \frac{\mu_0}{\mu} \nabla \times N \cdot H_s dv - \int_{\Omega_n} N \cdot j\omega\sigma A_s dv, \end{aligned} \tag{4}$$

where N is the linear combination of edge based shape functions, Ω_e the eddy current region, and Ω_n the current source region. The MATLAB biconjugate gradient stable function 'Bicgstab()' is used to solve the reduced A_e from discretised Equation (4). The sum of the freespace and reduced vector potential $A = A_s + A_e$ will be used for the sensitivity map calculation, which has been previously derived in [11]. With the (A, A) formulation and the usage of edge finite element, the Sensitivity matrix $(\frac{\delta V}{\delta \sigma})$ of the eddy current area can be calculated using dot product of electric fields [11], provided with equations $E = -j\omega A$. The sensitivity term between channel i and channel j for conductivity can be expressed as follows:

$$\frac{\delta V_{ij}}{\delta \sigma_k} = -\frac{\omega^2}{I_i I_j} \{A_i\} \left(\int_{\Omega_{ek}} \{N\} \cdot \{N\}^T dv \right) \{A_j\}^T. \tag{5}$$

Equation (5) gives us the sensitivity of the induced voltage pairs V_{ij} of coils of i, j with respect to an element, Ω_{ek} is the volume of element number k and I_i and I_j are excitation currents for the sensor i and sensor j respectively. With the new two potential methods with Biot-Savart implementation, forward model computation becomes faster, and the meshing process also becomes more straight forward, as coil structures do not need to be considered when creating the mesh. For low conductivity MIT measurement, the imaginary part of the sensitivity map will be used for image reconstruction.

3.2. Inverse Problem

The inverse problem for MIT is conversion of voltage measurements into a conductivity distribution image. The inverse problem in MIT is generally ill-posed and non-linear, which can be solved by many linear/non-linear inverse solvers [16–21]. However, solving a non-linear problem requires extensive computation of electromagnetic fields and updating the sensitivity maps [22]. Therefore, in most of the electrical tomography cases, linear responses are often presumed when reconstructing images using inverse solvers. This linear response assumption can simplify the non-linear problem to a linear approximation, where the problem can be solved through matrix multiplications. Given a linear response equation $\mathbf{Jx} = \mathbf{b}$, where $\mathbf{J}$ is the Jacobian matrix with size $m \times n$, $\mathbf{x}$ is the conductivity distribution and $\mathbf{b}$ is the sensor measurement changes, the least square Gauss Newton inverse solver with Tikhonov regularisation [23, 24] is to find the solution $\mathbf{x}$ which has the minimum error function:

$$\|\mathbf{b} - \mathbf{Jx}\|_2^2 + \|\mathbf{x} - \mathbf{x_0}\|_2^2. \tag{6}$$

If $\mathbf{x_0}$ is set to 0, the linear algebra in Equation (6) can be solved and rearranged to the following form

$$\mathbf{x} = \left(\mathbf{J}^\top \mathbf{J} + \lambda \mathbf{R}\right)^{-1} \mathbf{J}^\top \mathbf{b}, \tag{7}$$

where $\mathbf{R}$ is the regularisation matrix and λ the regularisation parameter. Choosing λ properly can effectively increase the system stability and remove the sharp edge from the reconstruction images, which results in a stable reconstructed object with smooth surface. In our two phase flow imaging experiments, two types of regularisation matrices were used: Tikhonov form and NOSER form. It is noted that NOSER form can generate a smoother image when the imaging object is located at the centre area. In Tikhonov form, $\mathbf{R}$ is an identity matrix, whereas in NOSER form, $\mathbf{R}$ is replaced by the diagonal elements of the matrix $(\mathbf{J}^\top \mathbf{J})$ [25].

In flow imaging, where there is movement involved in the imaging object, certain degrees of correlation exist between each consecutive image. In this case, the temporal algorithm can be implemented into the inverse solver to include the correlation information between the measurement frames. It is demonstrated that the temporal algorithm can effectively improve the noise performance and the stability of the images [26, 27]. Each temporal image is reconstructed based on the correlation between several images that are obtained using Equation (7). Introducing this temporal reconstruction makes MIT a suitable imaging technique for dynamic flow monitoring, since the additional information on dynamic behavior of underlying processes can be extracted.

4. EXPERIMENTAL RESULTS

To validate the feasibility of low conductivity two phase flow imaging using MIT, various configurations of conductivity distribution were tested and compared with the reconstructed images. To perform the experiments, saline solution with different concentrations were made: de-ionised water ($\sigma = 0\,\mathrm{S/m}$), 0.9% ($\sigma = 1.58\,\mathrm{S/m}$), 1% ($\sigma = 1.72\,\mathrm{S/m}$), 3% ($\sigma = 2.31\,\mathrm{S/m}$) and 5% ($\sigma = 7.26\,\mathrm{S/m}$) by weight. The saline solutions were contained in a 6 cm diameter plastic bottle and conductivity of the saline was measured by a Mettler Toledo Conductivity meter S_{30} at a temperature of 23°C. For the non-conductors tests, bottles filled with de-ionised water were used to simulate the non-conducting gas. All the experiments were completed within a relatively short period (less than 2 minutes), to avoid any other source of environmental variation. Figure 2 shows the normalised images of saline bottles (3% and 1% concentration) located at the centre of the imaging region, within a non-conductive freespace background.

Both Figures 2(a) and (b) show the location and size of the saline solution correctly. Although there is not much difference between the two images, it can be seen that the image of the 3% case has higher pixel values (see scaling bar), due to the higher electric conductivity of the 3% saline solution. Since the differential imaging and the linear inverse solver are used for image reconstruction, i.e., no absolute imaging can be achieved, the pixel values from the reconstructed image can only be used as a reference for the true conductivity values. In [6], an approximation equation is provided in the paper for the true permittivity calculation using a single channel measurement. It is therefore possible to realise the conductivity prediction using similar approaches for example a look up table or an approximation equation

provided that the sensor measurements are given. However, this is beyond the scope of the paper and will be investigated in the future study. The next experiment demonstrates the scenario of conducting objects inside a conductive background, which is achieved by inserting saline bottles into a saline background. Figure 3 shows the result images when the saline bottles (5% and 3%) are placed inside the imaging region with a 0.9% saline solution background.

Figure 3 also clearly shows the object location correctly in the reconstructed images. The difference between the 5% and 3% saline bottle can be distinguished very well from Figure 3(b). From the previous two experiments, both Figures 2 and 3 show reliable images as the conductivity contrast is still within an acceptable range. In the next experiment the non-conductive objects are placed within a 0.9% saline solution background, which further decreases the conductivity contrast (0 S/m and 1.58 S/m). Figure 4 shows the reconstructed images of non-conductive bottles sitting inside a 0.9% saline background.

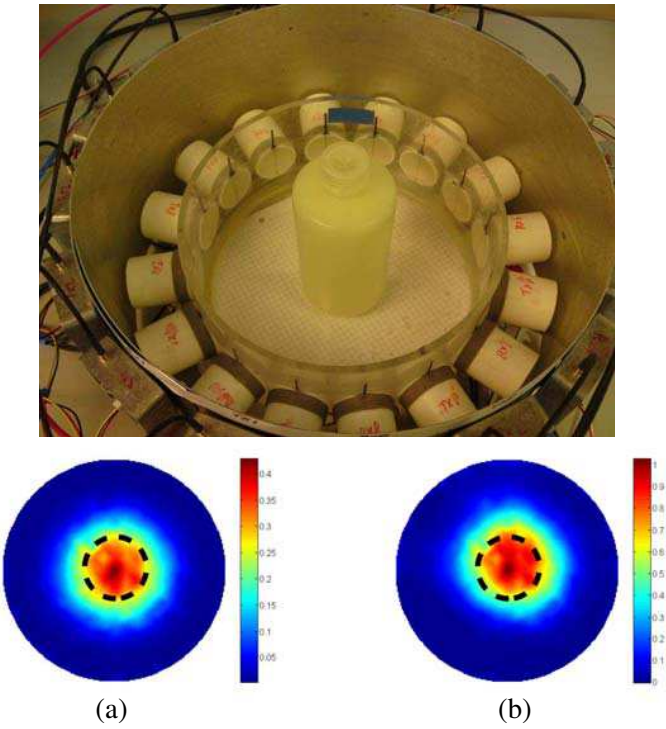

Figure 2. Reconstructed images of (a) one 1% saline bottle at the centre and (b) one 3% saline bottle at the centre.

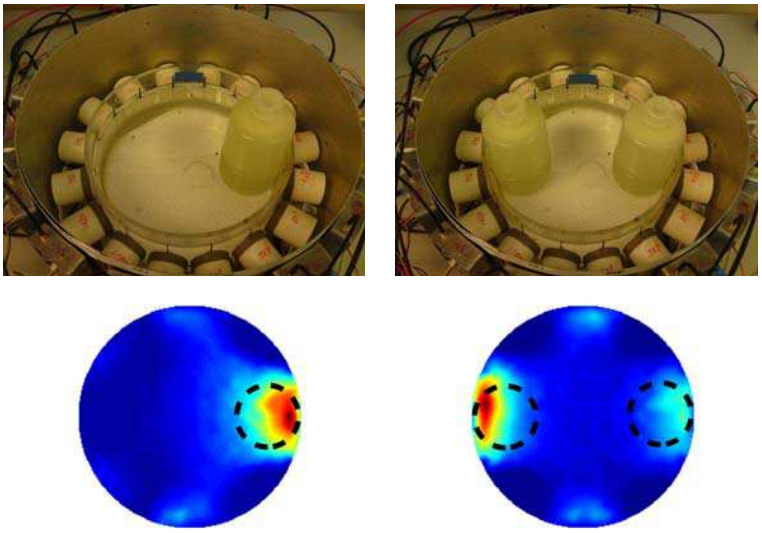

(a) (b)

Figure 3. The reconstructed images of (a) one 5% saline bottle located at the right hand side and (b) one 5% bottle at the left and one 3% bottle at the right.

The effect of low conductivity contrast is evident in Figure 4. Although the location and the size of the objects can still be identified, more noise is observed in the images because of the lower contrast, which results in blurring the images. To further represent the two phase flow imaging condition, another experiment was conducted to image various sizes of non-conducting bottles inside a conductive background. Seven different sizes of bottles were used, their diameters are as follows: 2.0 cm, 4.5 cm, 6.5 cm, 7.0 cm, 8.0 cm, 9.5 cm and 13 cm, which correspond to 31.9%, 17.1%, 12.1%, 9.3%, 6.8%, 3.8% and 0.76% of the total imaging area. The bottles were placed inside the measuring space in a size increment sequence. The images were all taken in series so the temporal algorithm can be applied to obtain the correlation information. The temporal method in theory should provide a smoother and more stable image. Figure 5 shows the snapshots from the temporally correlated images when the non-conductive bottles were placed at the centre and the side of the imaging space. To further determine the size error of the reconstructed images compared to the real situation, the image quality measurement are computed for each image. The term 'RES' is calculated using the quantification equations stated in [28] with a $\approx 40\%$ of the maximum scaling value as the threshold. If the calculated 'RES' is closer to 1, it

means that the reconstruction area is closed to the true dimension.

The increment of the bottle sizes can be clearly observed from the reconstructed images. Applying the temporal algorithm can effectively decrease the system noise during the conductivity variation process. In this experiment, since there is no variation of the conductivities of the insertion objects (0 S/m) and the background (1.58 S/m), the scaling of all the images have to remain the same in order to demonstrate the size increment. To quantify the area error, the 'RES' term is calculated for each image, it is shown that most of the RES value are within the acceptable range: $0.5 < \text{RES} < 1.5$. And the area error is shown to have a better performance when the bottles are placed at the side area, where has a higher sensitivity. The RES value can not be calculated for the 2.0 cm cases, because all the image pixels are smaller than the threshold value. However, the location of the 2.0 cm bottles can still be identified visually in the reconstructed images. The high sensitivity of the MIT system can thus be seen from these result images. The reconstructed images are able to pick up the smallest bottle used in the experiment (2 cm diameter), whose cross sectional area is about 0.72% of the entire measuring space. The system's sensitivity of detecting

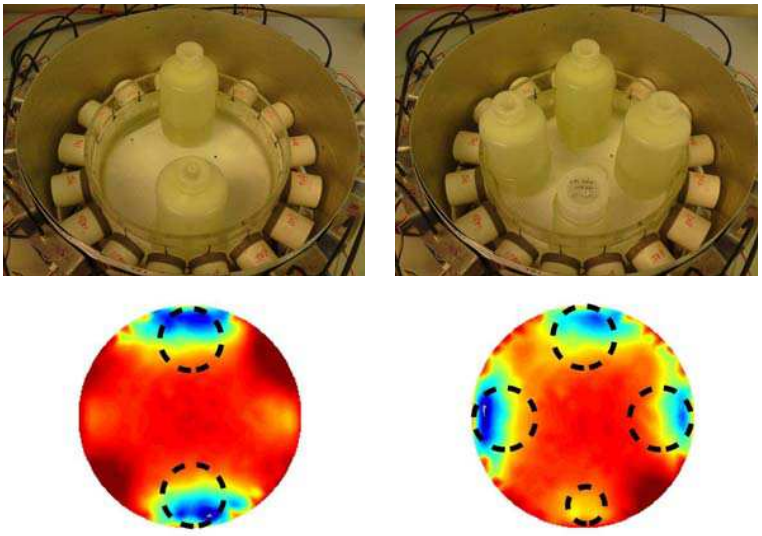

(a) (b)

Figure 4. The reconstructed images of (a) two non-conductive bottle located at the top and the bottom of the measuring space and (b) three 6 cm and one 2 cm diameter non-conductive bottles located evenly along the peripheral of the imaging space.

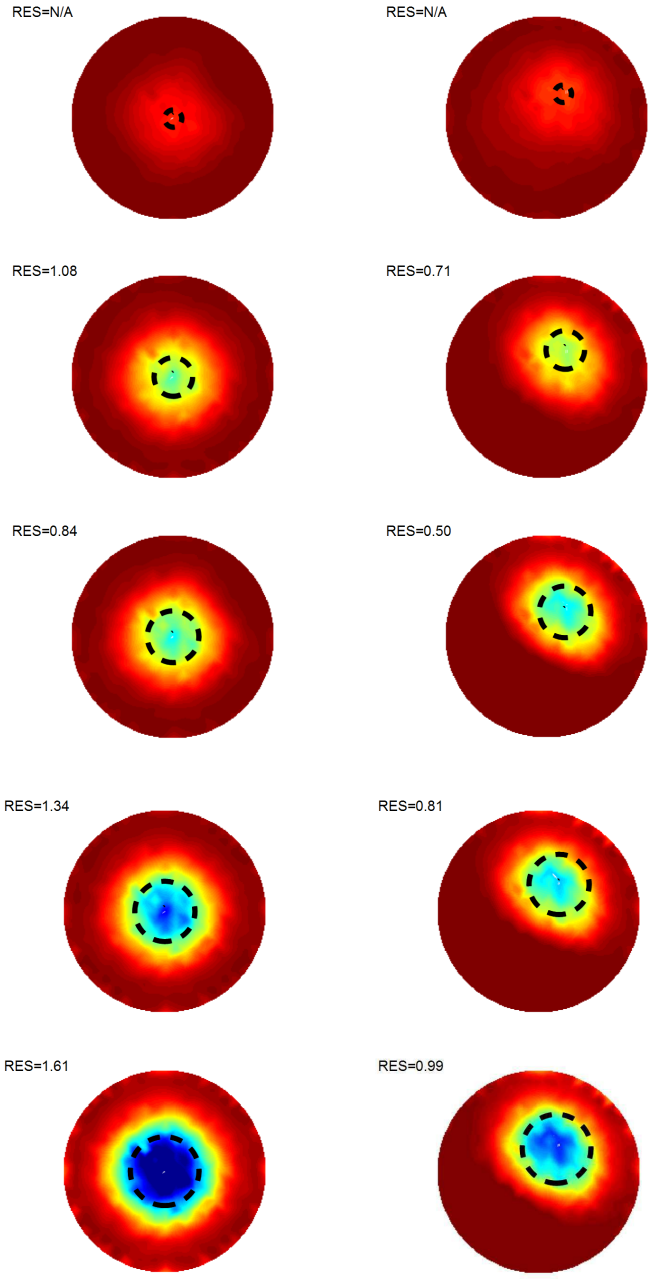
RES=N/A
RES=N/A
RES=1.08
RES=0.71
RES=0.84
RES=0.50
RES=1.34
RES=0.81
RES=1.61
RES=0.99

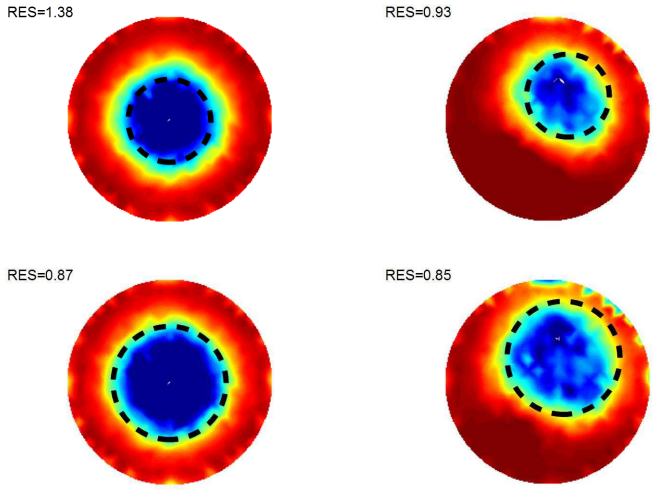

Figure 5. The reconstructed images of non-conductive bottles with various sizes inside a 0.9% conductive background. The non-conductive bottle was located at the (a) centre and (b) side of the region of interest.

a 1.58 S/m conductivity contrast in a less than 1% of imaging area is very promising and considered to be capable for the prospective two phase flow imaging application.

5. CONCLUSION

This paper presents the experimental verification for the potential usage of two phase flow monitoring using MIT technique. The non-contact feature of MIT system makes it a more suitable tool than EIT for imaging the low conductivity liquid/liquid or gas/liquid distribution. An MIT system that is capable of measuring low conductivity objects was designed and tested using several two phase imaging experiments. Although the detected perturbation signal has a very low magnitude due to the low conductivity contrast, our designed MIT system is still able to pick up the changes and produce useful images. From the hardware experiments, it was shown that the MIT system can produce images that clearly distinguish the locations of saline bottles with different conductivities. In the last result section of the paper (the size variation experiment), the designed system was able to pick up a tiny perturbation (1.58 S/m contrast) in a 0.72% portion of the whole imaging area. These temporal results are very satisfactory;

the changing bottle sizes can be visualised in the reconstructed images.

All these results have strengthened the possibility that MIT has potential to perform low conductivity two phase flow monitoring. It is a challenging task however, as there is still much work to be done, such as overcoming the sensitivity issue, system calibration setup and characterising the image regularisation. There is also room of improvement in terms of the hardware development. As stated before, a more precise mechanical construction can help eliminating various system error sources. However, with the prototype system, this paper has demonstrated the capability of MIT for low contrast conductivity imaging for industrial process tomography. In the future development, a dual modality system can be proposed by combining MIT with other type of imaging system, hence the reconstructed images can provide not only the conductivity distribution but the information of other passive electrical properties simultaneously.

REFERENCES

1. Griffths, H., "Magnetic induction tomography," *Institute of Physics Publishing Meas. Sci. Technol.*, Vol. 12, 1126–1131, Dec. 2001.
2. Ortiz-Aleman, C. and R. Martin, "Electrical capacitance tomography two-phase oil-gas pipe flow imaging by the linear back-projection algorithm," *Journal of Geophysics and Engineering*, Vol. 2, 32–37, 2005.
3. Kim, M. C., H. J. Lee, Y. J. Lee, and K. Y. Kim, "An experimental study of electrical impedance tomography for the two-phase flow visualization," *International Communications in Heat and Mass Transfer*, Vol. 29, No. 2, 193–202, 2002.
4. Terzija, N., W. Yin, G. Gerbeth, F. Stefani, K. Timmel, T. Wondrak, and A. J. Peyton, "Electromagnetic inspection of a two-phase flow of GaInSn and Argon," *Flow Measurement and Instrumentation*, Vol. 22, No. 3, 10–16, 2011.
5. Wondrak, T., S. Eckert, G. Gerbeth, K. Klotsche, F. Stefani, K. Timmel, A. J. Peyton, N. Terzija, and W. Yin, "Combined electromagnetic tomography for determining two-phase flow characteristics in the submerged entry nozzle and in the mold of a continuous casting model," *Metallurgical and Materials Transactions B*, Vol. 44, No. 6, 1201–1210, 2011.
6. Watson, S., R. J. Williams, W. A. Gough, and H. Griffths, "A magnetic induction tomography system for samples with

conductivities less than $10\,\mathrm{S/m}^{-1}$," *Measurement Science and Technology*, Vol. 19, 045501-11, 2008.

7. Liu, Z., M. He, and H. Xiong, "Simulation study of the sensing fileld in electromagnetic tomography for two-phase flow measurement," *Flow Measurement and Instrumentation*, Vol. 16, 199–204, 2005.
8. Wei, H. Y. and M. Soleimani, "Hardware and software design for a national instruments based magnetic induction tomography system for prospective biomedical applications," *Physiological Measurement*, Vol. 33, No. 5, 863–879, 2012.
9. Gursoy, D. and H. Scharfetter, "Imaging artifacts in magnetic induction tomography caused by the structural incorrectness of the sensor model," *Measurement Science and Technology*, Vol. 22, No. 1, 015502, 2011.
10. Soleimani, M., W. R. B. Lionheart, A. J. Peyton, and X. Ma, "A 3D inverse finite element technique applied to experimental magnetic induction tomography data," *4th World Congress on Industrial Process Tomography*, 1054–1059, Aizu, Japan, 2005.
11. Soleimani, M., "Sensitivity maps in three-dimensional magnetic induction tomography," *Insight No. 1*, Vol. 48, No. 1, 39–44, Jan. 2006.
12. Kameari, A., "Regularization on ill-posed source terns in FEM computation using two magnetic vector potentials," *IEEE Transaction on Magnetics*, Vol. 40, No. 2, 1310–1313, 2004.
13. Biro, O. and J. Preis, "On the use of the magnetic vector potential in the finite element analysis of three-dimensional eddy currents," *IEEE Transaction on Magnetics*, Vol. 25, No. 4, 3145–1359, 1989.
14. Biro, O., "Edge element formulations of eddy current problems," *Comput. Methods Appl. Mech. Engrg.*, Vol. 169, 391–405, 1999.
15. Biro, O. and K. Preis, "An edge finite element eddy current formulation using a reduced magnetic and a current vector potential," *IEEE Transaction on Magnetics*, Vol. 36, No. 5, 3128–3130, 2000.
16. Wei, H. Y. and M. Soleimani, "Three dimensional magnetic induction tomography imaging using a matrix free Krylov subspace inversion algorithm," *Progress In Electromagnetics Research*, Vol. 122, 29–45, 2012.
17. Goharian, M., M. Soleimani, and G. R. Moran, "A trust region subproblem for 3d electrical impedance tomography inverse problem using experimental data," *Progress In Electromagnetics Research*, Vol. 94, 19–32, 2009.

18. Flores-Tapia, D., M. O'Halloran, and S. Pistorius, "A bimodal reconstruction method for breast cancer imaging," *Progress In Electromagnetics Research*, Vol. 118, 461–486, 2011.
19. Ping, X. W. and T. J. Cui, "The factorized sparse approximate inverse preconditioned conjugate gradient algorithm for finite element analysis of scattering problems," *Progress In Electromagnetics Research*, Vol. 98, 15–31, 2009.
20. Liu, Z., Q. H. Liu, C. H. Zhu, and J. Yang, "A fast inverse polynomial reconstruction method based on conformal fourier transformation," *Progress In Electromagnetics Research*, Vol. 122, 119–136, 2012.
21. Tatarskii, V. I., "Use of semi-inversion method for the dirichlet problem in rough surface scattering," *Progress In Electromagnetics Research*, Vol. 54, 109–135, 2005.
22. Banasiak, R., R. Wajman, D. Sankowski, and M. Soleimani, "Three-dimensional nonlinear inversion of electrical capacitance tomography data using a complete sensor model," *Progress In Electromagnetics Research*, Vol. 100, 219–234, 2010.
23. Landesa, L., F. Obelleiro, J. L. Rodrguez, and M. R. Pino, "Stable solution of the GMT-MoM method by Tikhonov regularization," *Progress In Electromagnetics Research*, Vol. 20, 45–61, 1998.
24. Ma, L., H. Y. Wei, and M. Soleimani, "Pipeline inspection using magnetic induction tomography based on a narrowband pass filtering method," *Progress In Electromagnetics Research M*, Vol. 23, 65–78, 2012.
25. Cheney, M., D. Isaacson, J. C. Newell, S. Simske, and J. Goble, "NOSER: An algorithm for solving the inverse conductivity problem," *International Journal of Imaging Systems & Technology*, Vol. 2, 66–75, 1990.
26. Soleimani, M., C. N. Mitchell, and R. Banasiak, "Four-dimensional electrical capacitance tomography imaging using experimental data," *Progress In Electromagnetics Research*, Vol. 90, 171–186, 2009.
27. Wei, H. Y. and M. Soleimani, "Four dimensional reconstruction using magnetic induction tomography: Experimental study," *Progress In Electromagnetics Research*, Vol. 129, 17–32, 2012.
28. Adler, A., J. H. Arnold1, R. Bayford, A. Borsic, B. Brown, P. Dixon, T. J. C. Faes, I. Frerichs, H. Gagnon, Y. Garber, B. Grychtol, G. Hahn, W. R. B. Lionheart, A. Malik, R. P. Patterson, J. Stocks, A. Tizzard, N. Weiler, and G. K. Wolf, "Greit: A unified approach to 2D linear EIT reconstruction of lung images," *Physiological Measurement*, Vol. 30, No. 6, 35–55,

2009.

29. Banasiak, R., Z. Ye, and M. Soleimani, "Improving three-dimensional electrical capacitance tomography imaging using approximation error model theory," *Journal of Electromagnetic Waves and Applications*, Vol. 26, Nos. 2–3, 411–421, 2012.
30. Lai, J. C. Y., C. B. Soh, E. Gunawan, and K. S. Low, "Homogeneous and heterogeneous breast phantoms for ultra-wideband microwave imaging applications," *Progress In Electromagnetics Research*, Vol. 100, 397–415, 2010.
31. Bonafoni, S., F. Alimenti, G. Angelucci, and G. Tasselli, "Microwave radiometry imaging for forest fire detection: A simulation study," *Progress In Electromagnetics Research*, Vol. 112, 77–92, 2011.
32. Zhang, M., Y. W. Zhao, H. Chen, and W.-Q. Jiang, "SAR imaging simulation for composite model of ship on dynamic ocean scene," *Progress In Electromagnetics Research*, Vol. 113, 395–412, 2011.
33. Hajihashemi, M. R. and M. El-Shenawee, "Inverse scattering of three-dimensional PEC objects using the level-set method," *Progress In Electromagnetics Research*, Vol. 116, 23–47, 2011.
34. Catapano, I., F. Soldovieri, and L. Crocco, "On the feasibility of the linear sampling method for 3D GPR surveys," *Progress In Electromagnetics Research*, Vol. 118, 185–203, 2011.